Sinking city : The future of Bangkok amid Climate Change and Rising Sea Level

SEREE SUPHARATID

seree.s@rsu.ac.th

Rangsit University https://orcid.org/0000-0002-8036-4474

Sawitree Rojpratak

Rangsit University

Research Article

Keywords: Bias-correction, RQUANT, NGA, CMIP6, Flo-2D, QGIS

Posted Date: November 28th, 2025

DOI: https://doi.org/10.21203/rs.3.rs-8128112/v1

Sinking city : The future of Bangkok amid Climate Change and Rising Sea Level

Seree Supharatid[1,2*] and Sawitree Rojpratak[1,2]

[1]Climate change and disaster center, Rangsit University, Pathumthani 12000, Thailand
[2]College of Engineering, Rangsit University, Pathumthani 12000, Thailand

[*]Corresponding author : Seree Supharatid, Email seree.s@rsu.ac.th

Abstract

Bangkok and its metropolitan area (BMA) are highly vulnerable to compound flood hazards arising from both fluvial and coastal processes. This study investigates regional-scale compound flood impacts using a two-dimensional hydrodynamic model (Flo-2D) that integrates future climate projections from General Circulation Models (GCMs) under CMIP6 emission scenarios. Precipitation and river discharge were statistically downscaled and bias-corrected using the Robust Empirical Quantile Mapping (RQUANT) method. A Neuro-Genetic Algorithm (NGA) model was subsequently used to forecast river discharge, combining the adaptive learning capability of neural networks with the global optimization power of genetic algorithms. Results show that six-month monsoon precipitation is projected to increase by 3.92% (8.16%) and 12.72% (21.47%) under SSP2-4.5 (SSP5-8.5) by 2050 and 2100, respectively. Relative sea level rise further intensifies coastal flooding, with inundation areas projected to expand by 3.2% (3.6%), 8.2% (8.4%), 14% (15.1%), and 21.4% (26.2%) in 2030, 2050, 2070, and 2090, respectively. The findings highlight the inadequacy of the current national master plan in addressing compound flood risks. The interaction of intensified fluvial flooding and rising sea levels will amplify the severity and extent of future flood events. Strengthening adaptive urban planning, integrated water management, and early warning systems is essential to enhance Bangkok's resilience under future climate conditions.

Keywords Bias-correction, RQUANT, NGA, CMIP6, Flo-2D, QGIS

1 Introduction

As the world's urban population continues to grow, cities around the globe are increasingly exposed to the risks of flooding, causing 84% of natural disaster-related deaths (Jamali et al. 2020). One of the most pressing and complex flooding challenges facing urban areas today is compound flooding, namely pluvial (rainfall-induced), fluvial (river-induced), and coastal floodings. These can be caused by combination of hydrological, meteorological, astronomical, and climate factors (Gallien et al. 2011). This multifaceted flood event presents unique challenges for urban planners, policymakers, and residents, as the interactions between these different forms of flooding often amplify the overall impact, making mitigation and adaptation efforts far more difficult.

Urban areas are particularly vulnerable to compound flooding and flood risk will increase in the future due to their high population in the flood-prone areas, poorly-engineered flood control infrastructures, rapid urbanization, and climate change (Kirkpatrick and Olbert 2020). In pluvial flooding, intense rainfall overwhelms drainage systems that were not designed to handle such extreme events. This type of flooding is particularly concerning in cities, where stormwater drainage systems are unable to keep up with the growing frequency and intensity of heavy rainfall, often exacerbated by climate change. In parallel, fluvial flooding occurs when rivers overflow their banks due to sustained heavy rainfall upstream, melting snow, or other hydrological factors, inundating nearby urban areas that lie along riverbanks. Coastal cities are further at risk of coastal flooding, driven by rising sea levels, storm surges, and extreme weather events such as hurricanes or typhoons, all of which can bring seawater into the heart of the city.

The increasing of compound flooding risk in coastal cities is driven by 2 main factors: climate and land use changes. The Sixth Assessment Report of the Intergovernmental Panel on Climate Change (IPCC 2023) revealed that the global mean surface temperature for the present period (2011-2020) increased by 1.09 °C

from 1850 to 1900. The global mean sea level rose faster in the 20th century than in any prior century over the last 3 millennia, with a 0.20-m rise over the period 1901–2018.

General circulation models (GCMs) are essential tools in modern climate simulations, offering projections of future climate based on well-established physical principles (Randall et al. 2007). The latest CMIP6 models, regarded as state-of-the-art in climate modeling (Eyring et al. 2015), integrate both socioeconomic and climate change factors to deliver more comprehensive projections. However, most GCMs operate at coarse spatial resolutions (typically 100–300 km), which are inadequate for impact assessments requiring finer resolutions of only a few kilometers. For river basin scale, Krysanova et al. (2017) compared climate change impacts using nine regional-scale hydrological models paired with five GCMs under CMIP5 scenarios. Their study attributed uncertainties in annual mean flow projections to GCMs (57%), RCPs (27%), and hydrological models (16%). Kundzewicz et al. (2019) highlighted the challenges of obtaining reliable, detailed quantifications of past-to-present flood trends, noting that achieving similar accuracy for future projections is nearly impossible. These challenges stem from the lack of long-term, reliable flood-related data and the limitations of current climate models at finer scales. Nonetheless, various modeling tools and techniques have been developed to analyze flood inundation and address these knowledge gaps

Currently, urban flood risk studies based on scenario simulations primarily focus on assessing flood risk through inundation area and water depth (Olesen et al. 2017; Zhao et al. 2021). The simplistic bathtub model has been widely used to estimate coastal inundation, but it may underestimate the consequences of flooding due to its failure to account for river-tidal interactions (Lanzoni and Seminara 1998) and non-linear flood dynamics (Sanders 2017). In a broader context, mapping flood hazards in complex estuaries using methods that overlook local hydrodynamics can lead to underestimations of both flood extent and depth (FEMA 2015). While hydrodynamic modeling of rapid flood events in urban areas is a complex and challenging task, several successful studies on combined coastal-fluvial flooding have been conducted in recent years (Comer et al. 2017; Olbert et al. 2017; Gallien et al. 2018).

The Chao Phraya River Basin (CPRB), historically referred to as "Thailand's rice bowl," is home to approximately 40% of the country's population and contributes over 60% of its GDP. Consequently, it plays a vital role in Thailand's socioeconomic development, water management, and food security (Abhishek et al. 2021). However, the CPRB has frequently experienced devastating floods, such as those in 1995, 2006, and 2011. Numerous studies have analyzed the 2011 flood event (Komori et al. 2012; Sayama et al. 2015; Supharatid 2016; Budhathoki et al. 2022). This flood affected more than 13 million people between July and December, causing over 800 deaths (Komori et al. 2012). Kulp and Strauss (2019), using the CoastalDEM, projected a threefold increase in the number of people exposed to the high tide line by 2100 compared to projections using NASA SRTM DEM data. Even with significant carbon emission reductions, it is estimated that 17% of Thailand's population could face high tide lines exceeding their current land elevation by the end of the century. Hooijer and Vernimmen (2021) assessed the coastal flood risk using satellite LiDAR data and found that the biggest increases in inundation will occur after the first 2 meters of sea level rise, covering more than twice as much land as older elevation models predicted.

Bangkok, a critical area within the CPRB, is highly vulnerable to compound flooding. It's landscape and infrastructure are being increasingly threatened by both land subsidence and the escalating impacts of flooding. These issues, combined with rising sea levels, pose grave risks to the city's long-term sustainability and to the millions of people. Flooding has always been a challenge for Bangkok, a city that is built on a network of canals and rivers. The city's natural flood defenses, such as its wetland ecosystems and water management systems, have been strained by rapid urbanization, which has led to the loss of these natural buffers. Seasonal floods are now exacerbated by urban runoff, rising river levels, and the increasing frequency and severity of extreme weather events due to climate change. Combined with the sinking of the land, these floods have become more devastating, leading to widespread property damage, disruption of daily life, and economic losses.

Although some studies have analyzed compound flooding under climate change, there is a lack of research considering the combined effect of sea level rise (SLR) and future precipitation changes. This study aims to quantify flood extents and inundation over Bangkok and metropolitan area and evaluate adaptation measures under CMIP6 climate scenarios. We apply statistical bias correction and neuro genetic algorithm to analyze changes in precipitation and discharge from 18 GCMs. Subsequently, the Flo-2D model is employed to simulate the 2011 flood under a future climate. The impacts of sea level rise and changes in river discharge are examined through scenario-based simulations.

2 Study region : Chao Phraya river basin and big flood history

The Chao Phraya River Basin CPRB), our region of interest, is divided into the upper and lower CPRB (see Fig. 1). It is the largest river basin in the country, covering approximately 31% of Thailand's total area (162,800 km²). The upper CPRB comprises four main tributaries: the Ping River (watershed area: 33,900 km²), Wang River (10,800 km²), Yom River (23,600 km²), and Nan River (34,300 km²), all originating in the northern region. These rivers converge at Nakhon Sawan to form the Chao Phraya River, with the upper watershed spanning a total area of about 110,000 km². From Nakhon Sawan, the river flows through the lower basin, passing Ayutthaya and Bangkok before discharging into the Gulf of Thailand. The upper CPRB features mountainous terrain with steep slopes, while the lower CPRB is characterized by gentle slopes ranging from 1/10,000 to 1/15,000.

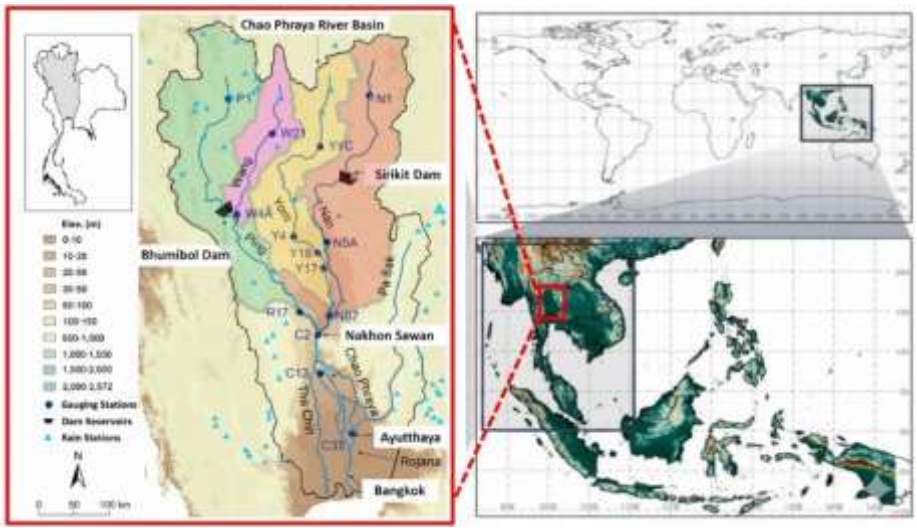

Fig. 1 Study area of CPRB

Generally, the flood behavior in the CPRB originates upstream, where rising water levels downstream lead to flooding across the floodplain. Additionally, water from tributaries often cannot flow into the Chao Phraya River due to its elevated water levels, resulting in overflow into the tributary floodplains. This phenomenon typically occurs in the lower watershed, where flooded areas naturally expand, causing significant damage to downstream locations along the river.

Severe flooding in the CPRB has become increasingly common over the past 20 years (see Fig. 2). The 2011 flood was the worst ever recorded in the country, surpassing even the damage caused by Hurricane Katrina (World Bank 2012). Continuous rainfall in the northern region accumulated nearly 1,675 mm of water, 42% higher than the 30-year average. This led to a significant runoff volume of more than 30,000 million cubic meters (mcm) passing through Nakhon Sawan Province, compared to approximately 27,000 mcm in the 2006 flood. Due to the limited capacity of the Chao Phraya and Pasak rivers, several riverbanks overflowed, and dykes along the rivers were breached, causing excessive flooding in several riverside communities and downstream areas.

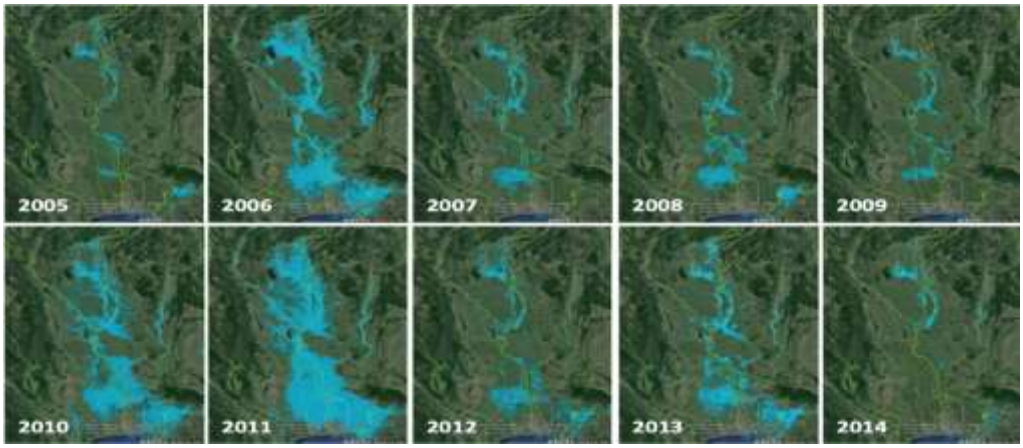

Fig. 2 Past 20-year severe floods in the CPRB (GISTDA)

Despite efforts to mitigate flood damage in the CPRB through structural measures such as dam construction, dikes, bypass canals, and pumping stations, flooding continues to cause significant impacts. This is largely due to deforestation, farmland expansion, and urban development. The increasing potential for flood damage is exacerbated by climate change, rapid urbanization, and extensive land development in downstream areas, particularly in Ayutthaya and other municipalities along the Chao Phraya River.

3 Data methodology

3.1 Observation datasets

Rainfall distribution in the CPRB is heavily influenced by the Asian summer monsoon, with distinct variations between the wet (May–October) and dry (November–April) seasons. Approximately 90% of the mean annual rainfall in the CPRB occurs during the wet season. Flooding typically occurs when wet-season precipitation exceeds 1,100 mm in this region.

In this study, we used the SA-OBS gridded precipitation dataset as a reference instead of station-based data, which are limited in both number and temporal coverage. Van den Besselaar et al. (2017) identified SA-OBS as the most reliable daily gridded observational dataset for the Southeast Asian (SEA) region. To maintain consistency and compatibility, we regridded the data to a 0.01° × 0.01° resolution using bilinear interpolation.

3.2 Model datasets

Eighteen models with varying resolutions from the CMIP6 database (accessible at https://esgf-node.llnl.gov/search/cmip6) were chosen for this study (see Table 1). CMIP6 builds upon CMIP5 by introducing updated specifications for concentration, emission, and land-use scenarios (Gidden et al. 2019) and revising the start year for future projections. In CMIP6, Shared Socioeconomic Pathways (SSPs) are combined with Representative Concentration Pathways (RCPs) to outline different socioeconomic trajectories (Riahi et al. 2017). For sea-level rise projections, regional data were sourced from the NASA Sea Level Projection Tool (Fox-Kemper et al. 2021; Garner et al. 2021). These datasets align with CMIP6 scenarios and are further detailed in Section 3.4.

To assess model performance and establish a baseline for evaluating future changes, we used historical simulations from the 1998–2014 period to represent the present-day climate. Future climate projections were analyzed under two scenarios: a medium-emission pathway (SSP2-4.5) and a high-emission pathway (SSP5-8.5). To ensure consistency, all models were regridded to a 0.01° × 0.01° resolution using the same bilinear interpolation method applied to the reference datasets.

Table 1 List of CMIP6 models used in this study

GCM	Research Center	Resolution
ACCESS-CM2	Australian Community Climate and Earth System Simulator	1.88°×1.25°
ACCESS-ESM1-5	Australian Community Climate and Earth System Simulator	1.88°×1.25°
BCC-CS°M2-MR	Beijing Climate Center, China Meteorological Administration, Beijing, China	1.12°×1.11°
CanESM5	Canadian Centre for Climate Modelling and Analysis, Environment and Climate Change Canada, Canada	2.81°×2.77°
CNRM-CM6-1	National Center for Meteorological Research, France	1.41°×1.39°
CNRM-ESM2-1	National Center for Meteorological Research, France	1.41°×1.39°
EC-Earth3	EC-Earth Consortium (EC-Earth)	0.70°×0.70°
FGOALS-g3	LASG, Institute of Atmospheric Physics, Chinese Academy of Sciences, Beijing, 100029, China	0.70°×0.70°
GFDL-ESM4	NOAA Geophysical Fluid Dynamics Laboratory, USA	1.25°×1.00°
INM-CM4-8	Institute for Numerical Mathematics, Russia	2.00°×1.50°
INM-CM5-0	Institute for Numerical Mathematics, Russia	2.00°×1.50°
IPSL-CM6A-LR	The Institut Pierre Simon Laplace, France	2.50°×1.27°
KIOST-ESM	Korea Institute of Ocean Science and Technology	1.89°×1.88°
MIROC6	JAMSTEC (Japan Agency for Marine-Earth Science and Technology, Japan), AORI (Atmosphere and Ocean Research Institute, The University of Tokyo), NIES (National Institute for Environmental Studies), and R-CCS (RIKEN Center for Computational Science), Japan	1.41°×1.39°
MIROC-ES2L	JAMSTEC, AORI, NIES, and R-CCS, Japan	2.81°×2.77°
MPI-ESM1-2-LR	Max Planck Institute for Meteorology, Germany	1.88°×1.85°
MRI-ESM2-0	Meteorological Research Institute, Japan	1.12°×1.11°
NESM3	Nanjing University of Information Science and Technology, China	1.88°×1.85°
NorESM2-LM	NorESM Climate modeling Consortium consisting of CICERO (Center for International Climate and Environmental Research), MET-Norway (Norwegian Meteorological Institute), NERSC (Nansen Environmental and Remote Sensing Center, Bergen), NILU (Norwegian Institute for Air Research), UiB (University of Bergen, Bergen), UiO (University of Oslo) and UNI (Uni Research), Norway	2.50°×1.89°

3.3 Bias correction

Several bias correction methods have been examined and applied in previous studies (Teutschbein and Seibert 2012; Supharatid et al. 2021), with Maraun (2016) providing a comprehensive review. Recently, machine learning (ML) and deep learning (DL) methods have shown outperform results against standard statistical methods like quantile mapping and quantile delta mapping (Zarei et al. 2021; Yoshikane et al. 2022; Li et al. 2023; Dhawan, et al. 2024).

In this study, a two-step methodology was implemented to improve bias correction and discharge forecasting from CMIP6 climate simulations.

In the first step, the nonparametric Robust Empirical Quantile (RQUANT) transformation method was applied using the *qmap* package in R (Gudmundsson et al. 2012; Gudmundsson 2016) to correct systematic biases in CMIP6 precipitation and discharge simulations. The RQUANT method employs local linear least-squares regression to estimate quantile–quantile relationships between observed and modeled time series at evenly spaced quantiles. Missing quantile values are interpolated from the fitted relationships to ensure continuity and robustness.

In the second step, a Neuro-Genetic Algorithm (NGA) was introduced as a hybrid machine learning approach for bias correction and discharge prediction. The NGA integrates the nonlinear approximation capability of neural

networks with the global optimization strength of genetic algorithms. Discharge was derived directly from total runoff flux (*mrro*) using an 18-model multi-model ensemble (MME). The NGA was then employed to forecast discharge based on the bias-corrected variables obtained from RQUANT. A schematic overview of the proposed methodology is presented in Fig. 3.

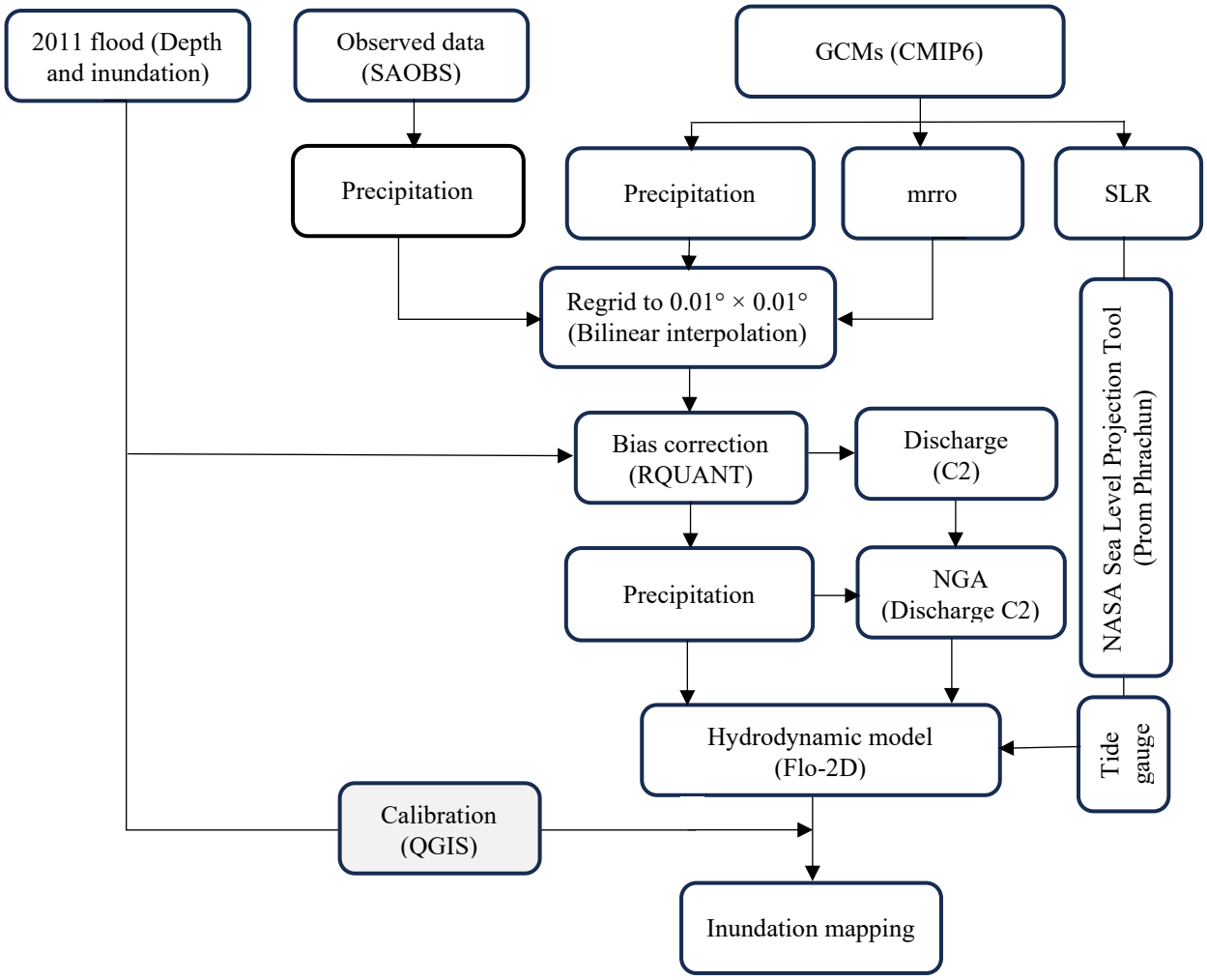

Fig 3 Schematic of the methodology proposed in this study

3.4 Flood simulation

Flood simulation provides a crucial foundation for effective flood mitigation and is essential for evaluating flood risk under both present and future conditions. The Flo-2D model, a two-dimensional flood routing system, simulates runoff across a grid of square elements while ensuring flow volume conservation. It numerically routes flood hydrographs, offering detailed insights into flood behavior. Key input parameters for the model include upstream flood hydrographs, spatial data on land use, elevation, soil properties, rainfall duration, and rainfall intensity, which are used to determine flood depths and inundation extents.

The Flo-2D software, developed by O'Brien et al. (1993), has been widely used in flood risk management, urban flood modeling, and simulations of mudflows and debris flows. It has been extensively applied to flood events in various studies (Luo et al. 2018; Mtamba et al. 2015; Dimitriadis et al. 2016). Some researchers have integrated the Flo-2D model with GCMs for flood mapping and impact assessments (Mishra et al. 2017; Hu et al. 2017; Erena et al. 2018; Kang et al. 2021). However, most studies have not accounted for compound factors related to climate change, such as extreme rainfall, sea level rise, and land subsidence. In this study, the Flo-2D model was employed to simulate flood inundation under present and future CMIP6

scenarios. The model is governed by two-dimensional equations, including the continuity equation (Eq. (2)) and momentum equations (Eqs. (3) and (4)).

$$\frac{\partial h}{\partial t} + \frac{\partial hU}{\partial x} + \frac{\partial hV}{\partial y} = e \tag{2}$$

$$S_{fx} = S_{ox} - \frac{\partial h}{\partial x} - \frac{U}{g}\frac{\partial U}{\partial x} - \frac{V}{g}\frac{\partial U}{\partial y} - \frac{1}{g}\frac{\partial U}{\partial t} \tag{3}$$

$$S_{fy} = S_{oy} - \frac{\partial h}{\partial y} - \frac{V}{g}\frac{\partial V}{\partial y} - \frac{U}{g}\frac{\partial V}{\partial x} - \frac{1}{g}\frac{\partial V}{\partial t} \tag{4}$$

where h is the flow depth, t is time, U and V are depth-averaged velocity components in the x and y directions, g is gravitational acceleration, and e represents excess rainfall intensity. The terms S_{fx} and S_{fy}, denote friction slopes, while S_{ox} and S_{oy}, represent bed slopes. Additional terms account for the pressure gradient, convective acceleration, and local acceleration, as shown in Eqs. (3) and (4).

The computational domain encompasses the CPRB, spanning from Nakhon Sawan to the Gulf of Thailand (Fig. 4). The flood hydrograph of 2011 is displayed on the right-hand side of the figure. For regional-scale flood simulation over the CPRB, unlike the Bathtub method (Kulp and Strauss, 2019), we use the Flo-2D model with a grid resolution of 1,000×1,000 m^2. The DEM was derived by merging the Shuttle Radar Topography Mission (SRTM, Version 2, http://dds.cr.usgs.gov/srtm/) for areas below 20 m. above mean sea level (msl) with CoastalDEM data for the downstream region. This approach enhances the simulation's accuracy in accounting for sea level rise near the Gulf of Thailand. Observed data, including rainfall, runoff, discharge, and cross-sections, were obtained from bias-corrected data described in Section 3.3 and from the Royal Irrigation Department. The 2011 flood event, recognized as one of the most severe flood in recent history, was used for model calibration. Six future flood simulations were conducted using projections based on CMIP6 emission scenarios. All simulations covered the peak monthly flood duration (October 1–31), consistent with the 2011 event.

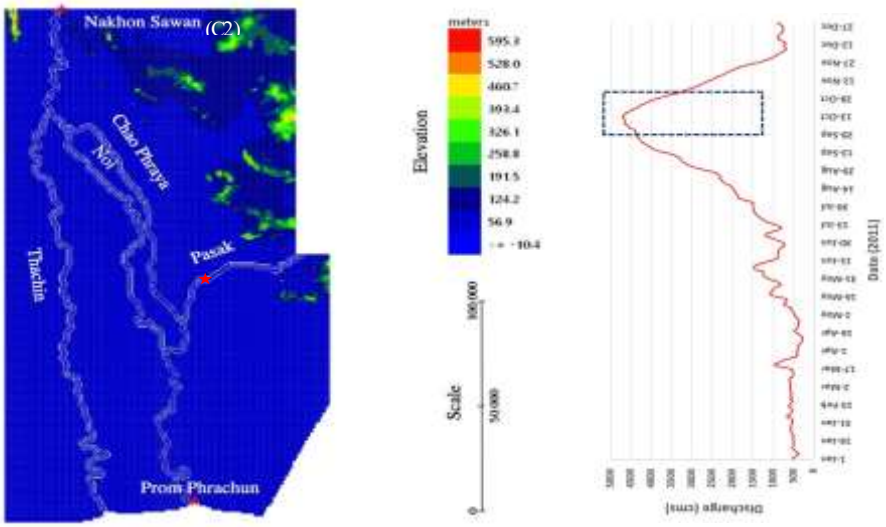

Fig. 4 Flo-2D model set-up and flood hydrograph

For the downstream boundary condition at Prom Phrachun, the total sea level rise relative to the baseline period (1998–2014) was used (see Fig. 5). Regional sea level rise contributions include sterodynamic sea level, glaciers, Greenland, Antarctica, land water storage, and vertical land motion. In the figure, thick lines represent median values, while shaded areas indicate the 17th–83rd percentile range. Three scenarios were considered: two medium-confidence scenarios (SSP2-4.5 and SSP5-8.5) and one low-confidence scenario (SSP5-8.5 low confidence), which accounts for the potential impacts of low-likelihood but high-impact ice sheet processes. Circles represent measured water levels from a gauge station; however, data after 2004 are incomplete (red dotted circles) due to station damage. To address this gap, data before 2004 were used to establish a linear trend for sea level rise. In this case, Line 2 (approximately 0.013 m/year) was chosen for forecasting regional sea level rise instead of Line 1 (approximately 0.021 m/year). The reduced slope of Line 2 is primarily attributed to a significant decrease in groundwater pumping following the implementation of groundwater management laws in 1997.

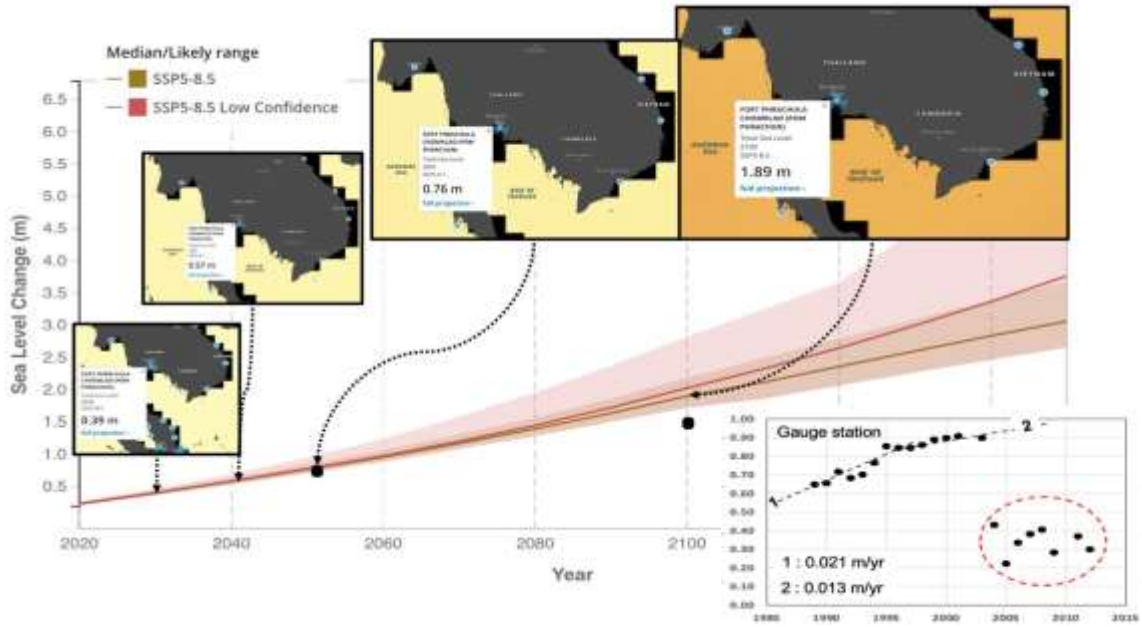

Fig. 5 Future relative sea level rise at sta. Prom Phrachun, Gulf of Thailand.
(Fox-Kemper et al. 2021; Garner et al. 2021)

4 Results and Discussions

4.1 Spatial change in precipitation

The spatial distribution of total precipitation on wet days (PRCPTOT) for SA-OBS and CMIP6 models over the upper and lower Chao Phraya River Basin is presented in Fig. 6. Significant overestimations in precipitation were observed in the BCC-CSM2-MR, CanESM5, INM-CM4-8, and INM-CM5-0 models, with INM-CM4-8 and INM-CM5-0 showing the highest precipitation levels. In contrast, some GCMs, including CNRM-CM6-1, CNRM-ESM2-1, EC-Earth3, and MPI-ESM1-2-LR, exhibited underestimations. Among these, the minimum precipitation levels were produced by the CNRM-CM6-1 and CNRM-ESM2-1 models.

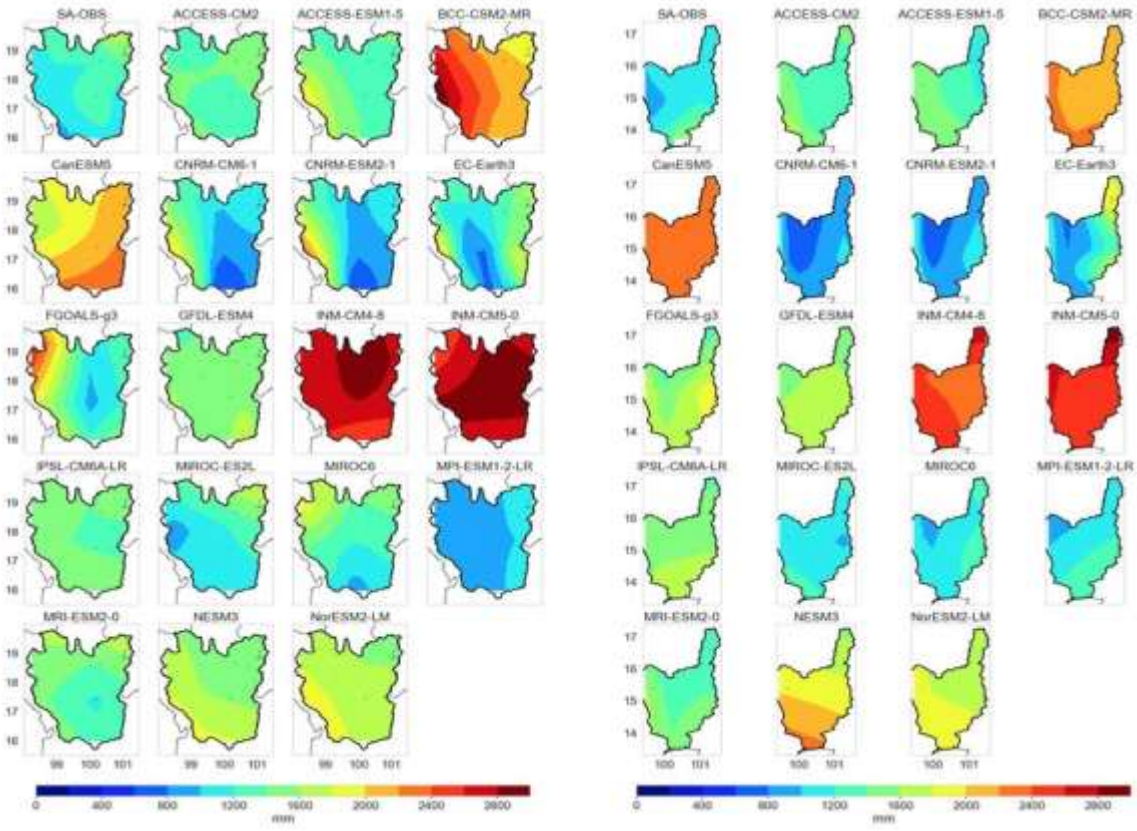

a) Upper CPRB

b) Lower CPRB

Fig. 6 Spatial distribution of precipitation over the CPRB

4.2 GCMs performance for projected changes in precipitation

In this study, 6-month precipitation data (May–October), the primary driver of flooding in the Chao Phraya River Basin (CPRB), were used to evaluate GCM performance. Precipitation data from SA-OBS for the upper and lower Chao Phraya basins were analyzed and used as reference values. A detailed intercomparison of CMIP6 models was conducted using the correlation coefficient (R), centered root mean-square difference (RMSD), and standard deviation (SD), which were visualized through a Taylor Diagram (Taylor 2001) for the reference period (see Fig. 7). Both RMSD and SD were normalized against their corresponding observations. Observations are represented by black symbols, while CMIP6 models, both before and after bias correction, are shown in various colors.

As observed in Fig. 5, models such as BCC-CSM2-MR, CanESM5, INM-CM4-8, INM-CM5-0, CNRM-CM6-1, and CNRM-ESM2-1 exhibited lower accuracy compared to other models. In general, most CMIP6 models before bias correction (represented by red and blue symbols) had correlation coefficients (R) ranging from 0.6 to 0.8, similar to the values obtained after bias correction (represented by green and pink symbols). This suggests that bias correction does not significantly enhance R. However, substantial reductions in RMSD and SD were observed following bias correction, indicating an overall improvement in model performance.

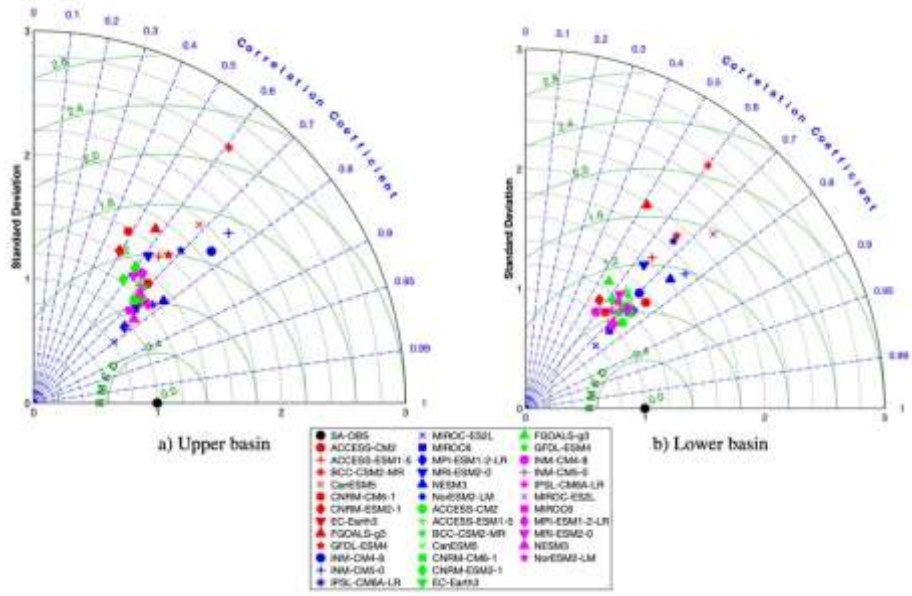

Fig. 7 Taylor diagram of 6-month precipitation
(Black : Observations, Red and Blue : Before bias correction, Green and Pink : After bias correction)

4.3 Temporal change in precipitation and discharge

The temporal changes in precipitation are illustrated in Fig. 8, which presents time series of 6-month precipitation (May–October) for the upper and lower CPRB from 2000 to 2100. The solid thick lines represent the 5-year running mean of the multi-model ensemble (MME), while the shaded regions indicate the minimum and maximum values from individual models. Precipitation over the upper CPRB is consistently higher than that over the lower CPRB. This is attributed to the forested and mountainous terrain in the upper CPRB, which leads to higher precipitation and evapotranspiration compared to the lower CPRB. Consequently, fluvial flood behavior has been a major concern during past floods and is expected to contribute to the frequency and magnitude of future floods. The projected precipitation exhibits a continuous increase over both the upper and lower CPRB, with greater magnitudes observed under the SSP5-8.5 scenario compared to the SSP2-4.5 scenario after 2050. In the upper CPRB, precipitation is projected to increase by 3.92% (8.16%) and 12.72% (21.47%) under SSP2-4.5 (SSP5-8.5) by 2050 and 2100, respectively. Similarly, in the lower CPRB, precipitation is expected to increase by 3.12% (8.36%) and 14.59% (17.80%) under SSP2-4.5 (SSP5-8.5) by the same years.

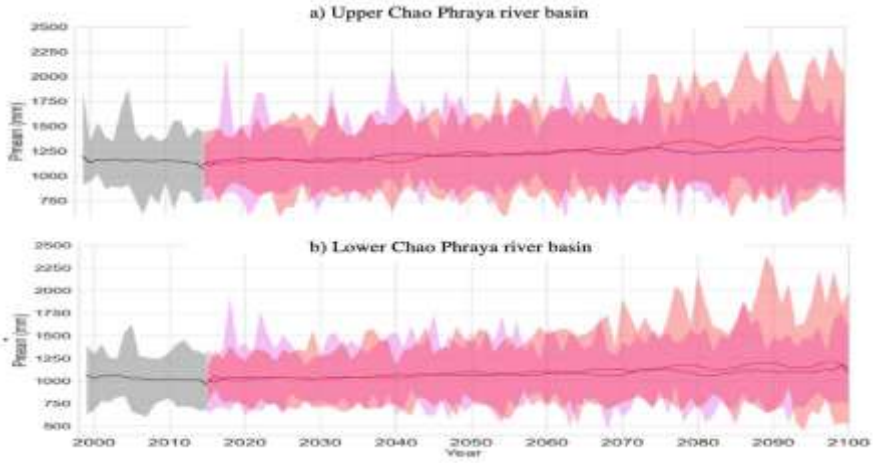

Fig. 8 Time series of 6-month precipitation (Black line and shed : MME and min. & max. of individual GCMs, during climatology, purple line and shed : MME and min. & max. of individual GCMs under SSP2-4.5, red line and shed : MME and min. & max. of individual GCMs under SSP5-8.5)

The projections of mean monthly precipitation over the upper and lower CPRB are shown in Fig. 9. The computed results for the reference period (June to August) exhibit an overestimation compared to observed values. Under the SSP5-8.5 scenario, a significant increase in precipitation during August was found over the upper CPRB, with projected increases of 0.66%, 6.7%, and 10.55% for the near-, mid-, and far-future periods, respectively.

a) Upper Chao Phraya river basin

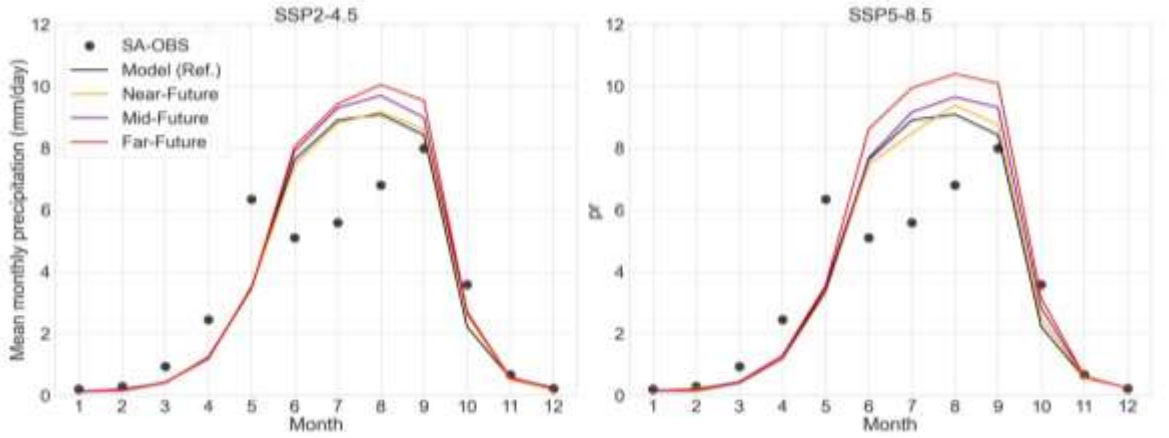

b) Lower Chao Phraya river basin

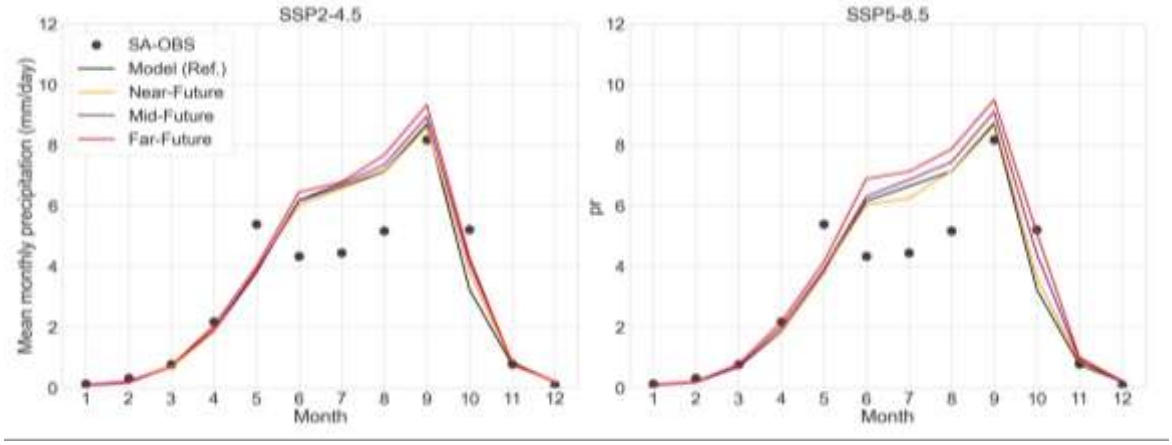

Fig. 9 Projected mean monthly precipitation over the upper and lower CPRB

For discharge projections, the climate model outputs were directly utilized following the approach of St. Jacques et al. (2018). The total runoff flux (*mrro*) from the 18-model multi-model ensemble (MME) was converted into discharge by aggregating the upstream grid-cell values contributing to station C2. The resulting mean-monthly discharge was subsequently bias-corrected using the method described in Section 3.3.

For the Neuro-Genetic Algorithm (NGA) model, the climatological dataset was divided into two subsets: 80% for training and 20% for testing. The input variables comprised mean-monthly precipitation from the Ping, Wang, Yom, and Nan river basins, along with concurrent discharge at station C2 (see Fig. 1). The output variable was the one-month-ahead discharge at the same station.

Figure 10 presents the time series and scatter plots of monthly discharge during the training and testing phases. Evaluation metrics, including the root mean square error (RMSE) and the coefficient of determination (R^2), are shown in the figure. Results indicate that the NGA model substantially reduces mean bias (in terms of RMSE), enhances the representation of extreme discharge values, and effectively captures temporal

variability. The model exhibited strong agreement with observed data, achieving R^2 values of 0.65 and 0.85 for the training and testing datasets, respectively.

Based on its superior performance (Fig. 10), the NGA model was employed to project future monthly discharge under the SSP2-4.5 and SSP5-8.5 emission scenarios (Fig. 11). The mean-monthly discharge for target years (2030, 2050, 2070, and 2090) was computed by averaging the ten years before and after each period. Results suggest a consistent increase in discharge across all future timeframes, particularly under high-emission conditions. The mean discharge at station C2 is projected to increase by 20% (25%), 27% (28%), 35% (40%), and 39% (51%) under the SSP2-4.5 (SSP5-8.5) scenarios by 2030, 2050, 2070, and 2090, respectively.

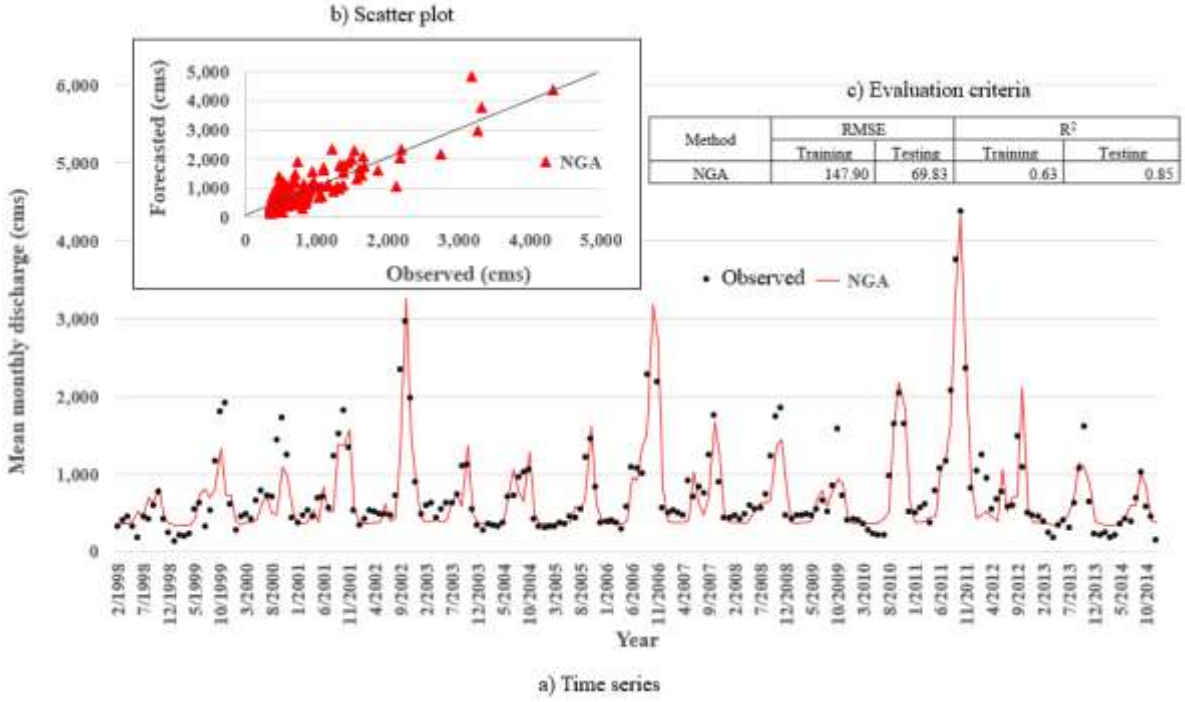

Fig. 10 Time series of monthly discharge at sta. C2 (Circles : Observation, Red line : NGA) during climatology

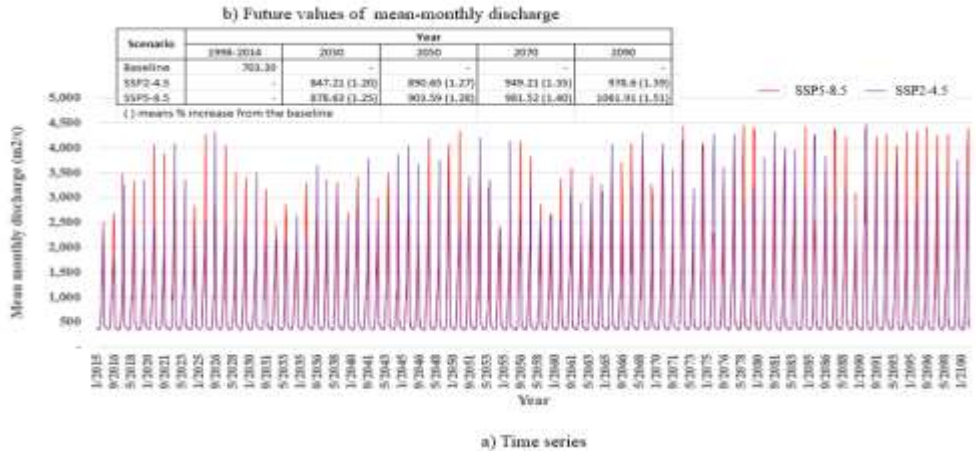

Fig. 11 Time series of projected monthly discharge and mean-monthly discharge at target year (2030, 2050, 2070, and 2090) under SSP2-4.5 and SSP-5-8.5

4.4 Assessment of flood depth and flood inundation area of the 2011 flood

This study employs 1,000 x 1,000 m^2 square grids for regional-scale flood modeling, consistent with the downscaled GCM and reference dataset (SA-OBS) for 1-month simulations (October). The Flo-2D model was first used to simulate the 2011 flood, with Manning's n calibrated (via trial and error) to match the observed water levels and discharge. Figure 12 illustrates the time series of maximum water levels at three stations (C3, C7A, and C4) along the Chao Phraya River during the 2011 flood. The simulated maximum water levels are higher than observed values, potentially due to unaccounted upstream dike failures of station C3 in the model.

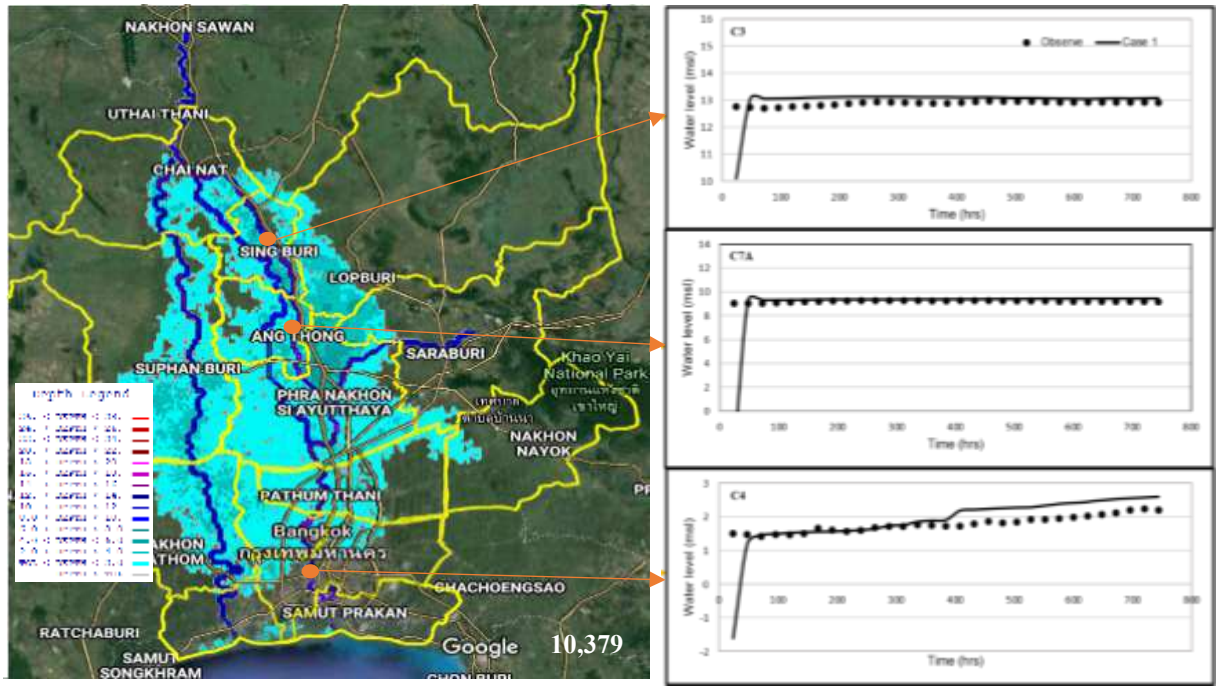

Fig. 12 Time series of the maximum water level at 3 stations (C3, C7A, and C4) for 2011 flood

To analyze inundation areas, a satellite image (Fig. 13a) of the Chao Phraya Basin flood from the Radio Amateur Society of Thailand was utilized. As the image lacked georeferenced information, geographic reference coordinates were assigned by selecting clear Ground Control Points (GCPs) and matching them to real-world coordinates using QGIS. The Identify Feature tool was employed to extract the RGB (Red, Green, and Blue) intensity values of flood pixels, and the Raster Calculator defined a formula to classify RGB values corresponding to flood areas as "1" and non-flood areas as "0." The Zonal Histogram tool (Fig. 14) analyzed raster values to determine the number of flood grids, and the total flood area was calculated based on grid size (QGIS Development Team, n.d.). Figure 15 displays the flooded areas on October 31, 2011 derived from the satellite image (Fig. 15a), the FLO-2D model (Fig. 15b), and the overlay picture (Fig. 15c). The flooded areas from the FLO-2D model and the satellite image were calculated as 10,686 km^2 and 9,833 km^2, respectively (8.6% difference). More advance of flood extent was observed from the model than the satellite image. This is caused by the unaccounted upstream dike failures of the model mentioned earlier.

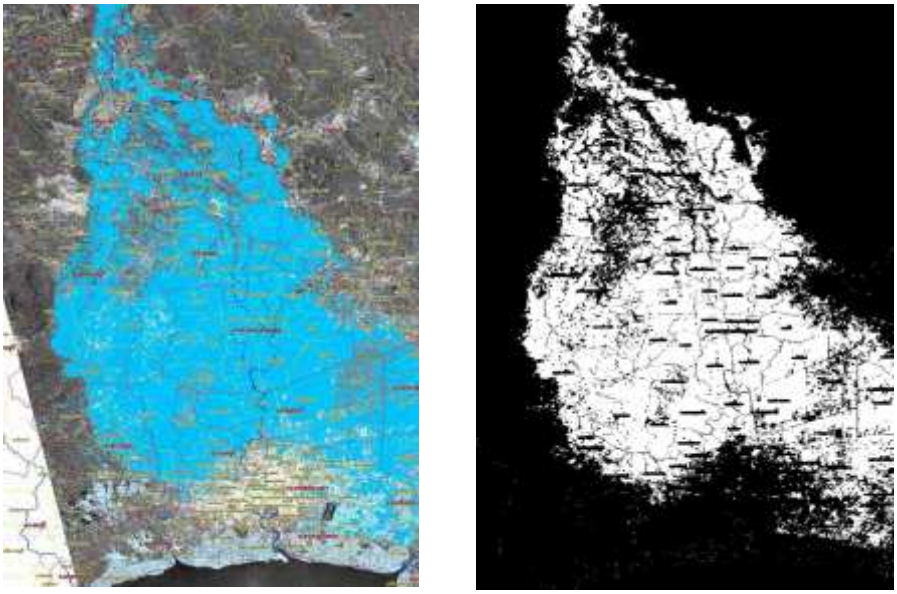

a) Flood area on October 30, 2011

b) Flood area in QGIS (white) and non-flood areas (black)

Fig. 13 Flood areas on October 30, 2011

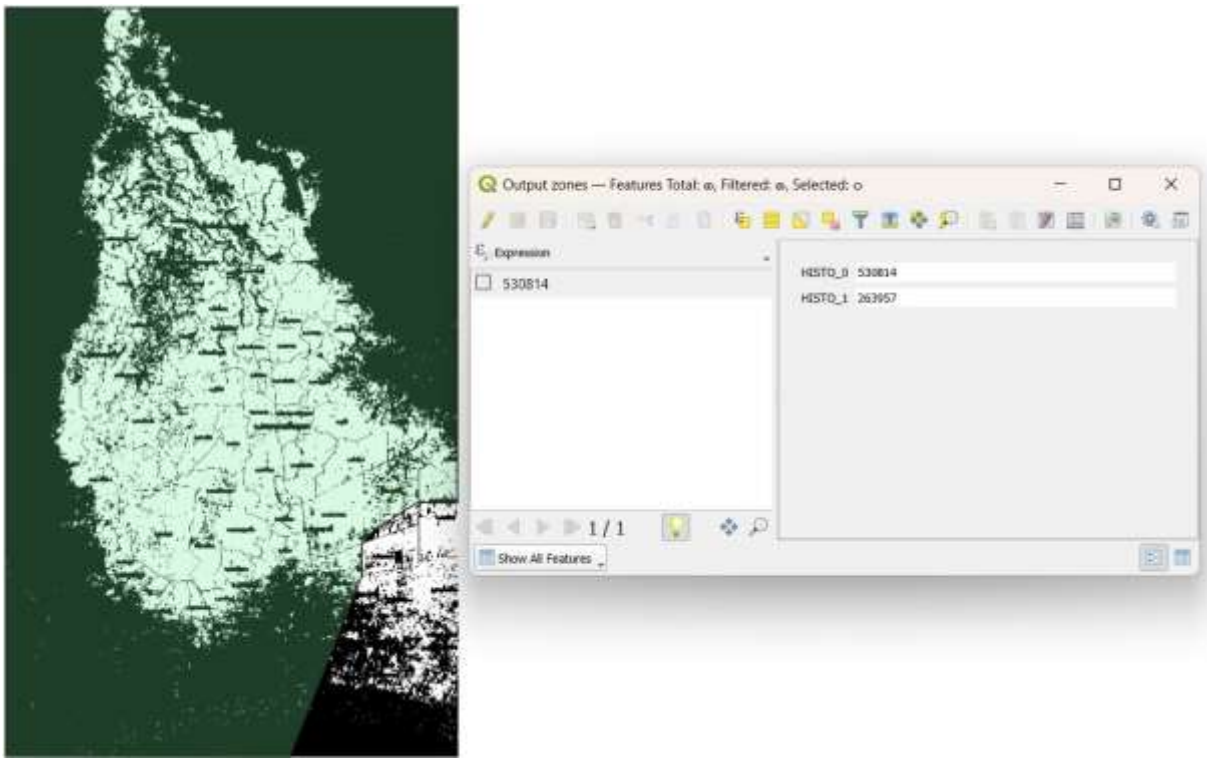

Fig. 14 The Zonal Histogram command generates a table showing the number of flooded grids (HISTO_0) and non-flooded grids (HISTO_1), calculated specifically for the Chao Phraya Basin area (green zone).

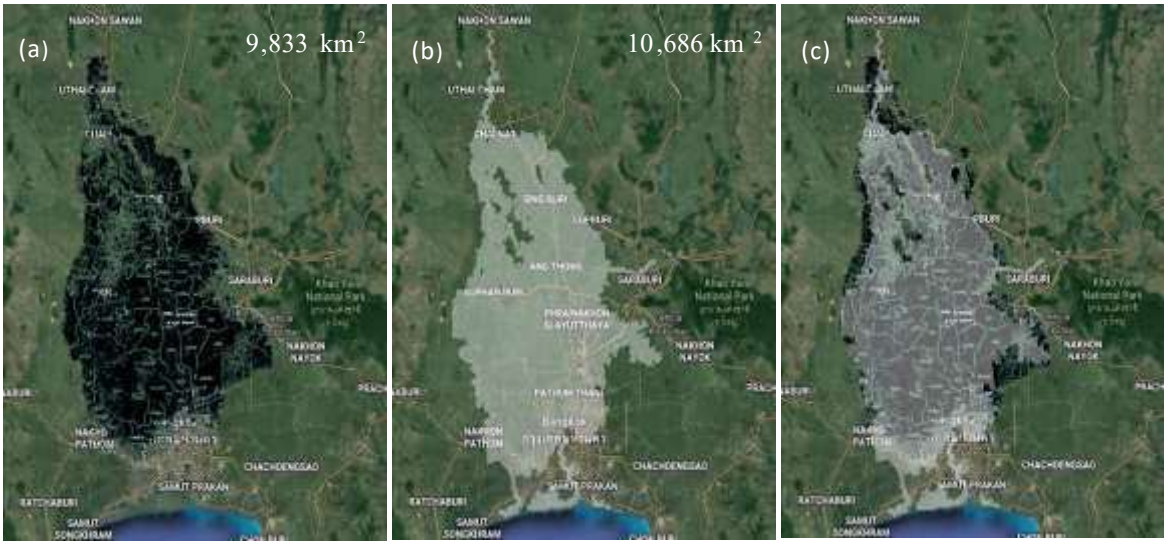

Fig. 15 Comparison of flood areas (a) Flood areas on October 31, 2011, b) Flood areas identified from satellite imagery, and c) an overlay picture)

4.5 Projected maximum flood inundation depth and area with adaptation measures

Under the SSP2-4.5 and SSP5-8.5 scenarios, the Flo-2D model was applied with MME forcing outputs, including increased precipitation and sea-level rise. Major adaptation measures under the national master plan, incorporating three bypass channels (Measures 2.2, 3, and 7; see Fig. 16), were evaluated under a future climate. The design capacities of the bypass channels are 500, 500, and 1,200 cms, respectively.

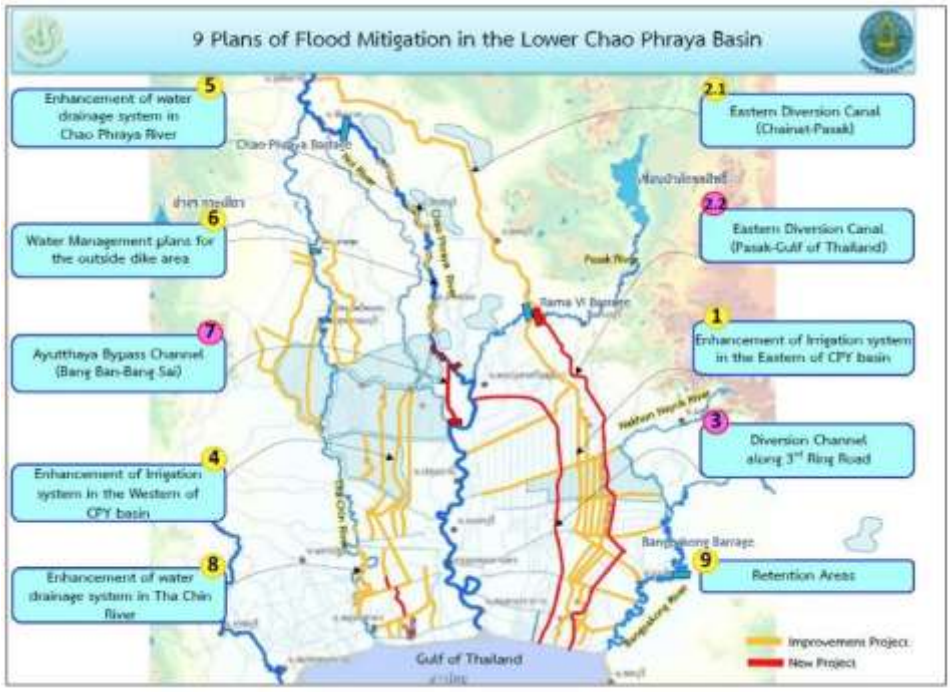

Fig. 16 Flood mitigation plan for the lower CPRB (Irrigation department, 2017)

This study focuses on simulating the flood behavior of the 2011 event under future climate conditions. Figure 17 illustrates the projected maximum flood inundation depth and extent under SSP2-4.5 and SSP5-8.5 scenarios, incorporating the adaptation measures shown in Figure 16**.** The corresponding inundation areas (in km²) are indicated in the lower-right panel of the figure.

With major adaptation measures in Fig. 16, the 2011 flood inundated area is reduced by 357 km^2 (3.4%). Results also suggest that, relative to the 2011 flood, the inundated area is projected to increase by 3.2% (3.6%)**,** 8.2% (8.4%)**,** 14% (15.1%)**,** and 21.4% (26.2%) in 2030, 2050, 2070, and 2090, respectively, under SSP2-4.5 (SSP5-8.5). Spatiotemporal analysis indicates an upstream migration of fluvial flooding and a downstream expansion of coastal flooding toward Bangkok and its metropolitan area (BMA**)** between 2030 and 2090.

Despite the implementation of the national master plan presented in Figure 16, large-scale flooding in the lower CPRB, particularly across the BMA, appears unavoidable under future high-emission conditions. These findings highlight the need for additional adaptation measures, including both small- and large-scale nature-based solutions (NbS) in the upper and lower CPRBs, to mitigate future flood severity and enhance long-term resilience.

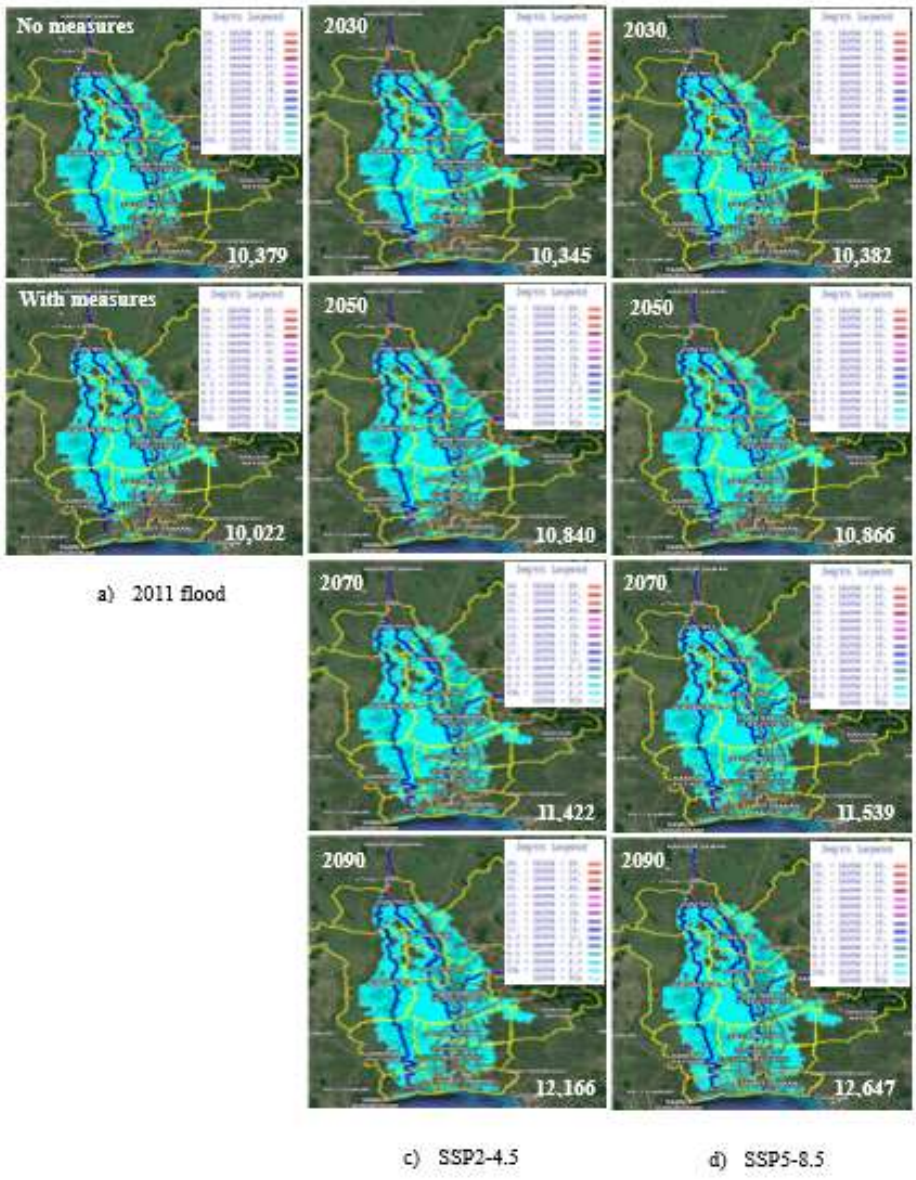

Fig. 17 Projected maximum flood inundation depth and area under SSP2-4.5 and SSP5-8.5 emission scenarios with adaptation measures

5 Summary and Conclusions

The Chao Phraya River Basin (CPRB), covering nearly one-third of Thailand's total land area, has long supported agricultural productivity through its seasonal flooding regime. However, under a changing climate, the spatial extent and frequency of flood-prone areas have increased substantially. With rapid urban expansion and intensified land use, the prevention and mitigation of flood risks have become increasingly critical. The 2011 flood event, one of the most devastating in Thailand's history, affected more than 13 million people, resulted in over 800 fatalities, and caused an estimated economic loss of approximately USD 45.7 billion**.**

In this study, the nonparametric Robust Empirical Quantile (RQUANT) transformation method, implemented in the *R* software package qmap, was employed to correct systematic biases in CMIP6 simulations of precipitation and discharge. Rather than relying on station-based observations, the grid-based SA-OBS precipitation dataset was used as the reference for bias correction. River discharge was derived directly from the total runoff flux (mrro) provided by an 18-model multi-model ensemble (MME). Subsequently, a Neuro-Genetic Algorithm (NGA) model was introduced as a hybrid machine learning framework to forecast river discharge, integrating the representational learning capacity of neural networks with the global optimization capability of genetic algorithms. The key findings derived from this approach are summarized below.

Overall, for precipitation, most CMIP6 models exhibited correlation coefficients (R) ranging from 0.6 to 0.8 prior to bias correction, with values remaining largely unchanged after correction. This indicates that the bias correction process does not substantially enhance the correlation structure of individual models. However, the root mean square deviation (RMSD) and standard deviation (SD) were markedly reduced following correction, demonstrating a significant improvement in the overall performance and reliability of the CMIP6 simulations.

The projected six-month monsoon precipitation exhibits a consistent increasing trend across both the upper and lower CPRB, with greater magnitudes under the SSP5-8.5 scenario compared to SSP2-4.5. Precipitation in the upper CPRB is generally higher than in the lower basin, primarily due to extensive forest cover and mountainous terrain, which enhance orographic rainfall and evapotranspiration. Consequently, fluvial flooding remains a major concern, as observed in previous extreme flood events. Specifically, precipitation in the upper CPRB is projected to increase by 3.92% (8.16%) and 12.72% (21.47%) under SSP2-4.5 (SSP5-8.5) for the years 2050 and 2100, respectively. Corresponding increases in the lower CPRB are 3.12% (8.36%) and 14.59% (17.80%), indicating a basin-wide intensification of precipitation extremes under future climate scenarios.

The simulated discharge was substantially improved through the application of the Neuro-Genetic Algorithm (NGA) model, demonstrating enhanced accuracy and reduced bias relative to the reference dataset. The projected discharge at station C2 exhibits a persistent increasing trend throughout the 21st century, with pronounced rises during the far-future period. Specifically, discharge is projected to increase by 20% (25%), 27% (28%), 35% (40%), and 39% (51%) under the SSP2-4.5 (SSP5-8.5) scenarios for the years 2030, 2050, 2070, and 2090, respectively, relative to the historical baseline. These findings indicate a progressive intensification of river flow, particularly under high-emission scenarios.

Unlike the simplified bathtub approach, the FLO-2D hydrodynamic model was employed to simulate regional-scale compound flooding across the CPRB. Bias-corrected outputs from the CMIP6 multi-model ensemble (MME) under the SSP2-4.5 and SSP5-8.5 scenarios served as inputs for the simulations. The 2011 Thailand Great Flood event was reproduced for model calibration. The simulated maximum water levels were slightly higher than the observed values, primarily attributed to the omission of dike failures in the upstream regions. Using QGIS, flood inundation extents derived from satellite imagery were compared with model results. The FLO-2D simulation estimated an inundation area of 10,686 km², closely matching the satellite-derived extent of 9,833 km², thereby confirming the model's reliability for large-scale flood assessment.

The FLO-2D model was further employed under the SSP2-4.5 and SSP5-8.5 scenarios to assess the effectiveness of adaptation measures outlined in Thailand's National Master Plan, which includes the construction of three major bypass channels. Simulation results indicate that the projected maximum inundation area will increase by 3.2% (3.6%)**,** 8.2% (8.4%)**,** 14% (15.1%)**,** and 21.4% (26.2%) in 2030**,** 2050**,** 2070, and 2090, respectively, relative to the 2011 baseline flood. Despite the implementation of these

structural measures, severe flooding in the lower CPRB, particularly across Bangkok and its metropolitan area remains highly probable. These findings highlight the need for complementary strategies, particularly the integration of small- and large-scale nature-based solutions (NBS) across both the upper and lower CPRB, to enhance resilience and mitigate future flood severity.

In conclusion, this study underscores the escalating flood risk in the Bangkok Metropolitan Area (BMA) driven by projected increases in both precipitation and sea level rise, which collectively heighten the city's exposure and vulnerability. The socio-economic consequences are expected to be most severe for low-income communities, who have limited adaptive capacity. When compounded by ongoing land subsidence, these factors are likely to exacerbate flood hazards substantially. Although flood protection infrastructure and management strategies across the Chao Phraya River Basin (CPRB) have improved since the 2011 flood, they remain insufficient to cope with the complexity of compound flooding events. Without the implementation of robust, long-term policy interventions and adaptive measures, particularly those addressing sea level rise and land subsidence, flood risks in BMA are projected to intensify in the coming decades.

Author contributions

Seree Supharatid : Supervision, Conceptualization, Methodology, Modeling experiments, Resources, Writing – review & editing. Sawitree Rojpratak : Conceptualization, Methodology, Modeling experiments, Analysis, Visualization, Writing original draft.

Funding

The authors gratefully acknowledge the support of the Thailand Research Fund (The Royal Golden Jubilee Ph.D. Program) for providing a full scholarship under grant number PHD/0203/2560.

Acknowledgements

We sincerely appreciate the anonymous reviewers for their valuable feedback. We also extend our thanks to the Earth System Grid Federation (ESGF) for archiving and granting access to the CMIP6 dataset, as well as to the providers of the observational datasets cited in this manuscript.

Conflict of interest

The authors declare that they have no conflict of interest with regard to this article.

Data availability Statement

The CMIP6 data were downloaded from the WCRP Earth System Grid Federation (ESGF) website (https://esgf-node.llnl.gov/projects/cmip6/). SA-OBS data are freely available online (https://sacad.database.bmkg.go.id/download/grid/download.php). Analysis (Downscaling and bias-corrected) data used during the study are available from the corresponding author by request.

Orcid

Seree Supharatid https://orcid.org/0000-0002-8036-4474

References

Abhishek, Kinouchi T, & Sayama T (2021) A comprehensive assessment of water storage dynamics and hydroclimatic extremes in the Chao Phraya River Basin during 2002–2020. Journal of Hydrology, 603, 126868.

Budhathoki A, Tanaka T, & Tachikawa Y (2022) Correcting streamflow bias considering its spatial structure for impact assessment of climate change on floods using d4PDF in the Chao Phraya River Basin, Thailand. Journal of Hydrology: Regional Studies, 42, 101150. https://doi.org/10.1016/j.ejrh.2022.101150

Comer J, Olbert AI, Nash S, Hartnett M (2017) Development of high-resolution multi-scale modelling system for simulation of coastal-fluvial urban flooding. Nat. Hazards Earth Syst. Sci. 17, 205–224. https://doi.org/10.5194/nhess-17-205-2017.

Dhawan T, Torre DD, Niazkar M, Kaffas K, Larcher M, Righetti M, Menapace A (2024) A comprehensive comparison of bias correction methods in climate model simulation : Application on ERA-5 Land across different temporal resolutions, Heliyon, https://doi.org/10.1016/j.heliyon.2024.e40352

Dimitriadis P, Tegos A, Oikonomou A, Pagana V, Koukouvinos A, Mamassis N, Koutsoyiannis D & Efstratiadis A (2016) Comparative evaluation of 1D and quasi-2D hydraulic models based on benchmark and real-world applications for uncertainty assessment in flood mapping. Journal of Hydrology, 534, 478-492.

Erena SH, Worku H, & De Paola F (2018) Flood hazard mapping using FLO-2D and local management strategies of Dire Dawa city, Ethiopia. Journal of Hydrology: Regional Studies, 19, 224-239. https://doi.org/10.1016/j.ejrh.2018.09.005

Eyring V, Bony S, Meehl GA, Senior CA, Stevens B, Stouffer RJ, & Taylor KE (2015) Overview of the Coupled Model Intercomparison Project Phase 6 (CMIP6) experimental design and organization. Geoscientific Model Development, 9(5), 1937-1958. https://doi.org/10.5194/gmdd-8-10539-2015

FEMA (2015) Guidance and standards for flood risk analysis and mapping. Combined coastal and riverine mapping (No Guidance Document 22). FEMA.

Fox-Kemper B, HT Hewitt, C Xiao, G Aðalgeirsdóttir, SS Drijfhout, T L Edwards, NR Golledge, M Hemer, RE Kopp, G Krinner, A Mix, D Notz, S Nowicki, IS Nurhati, L Ruiz, JB. Sallée, ABA Slangen, Y Yu (2021) Ocean, Cryosphere and Sea Level Change. In: Climate Change 2021: The Physical Science Basis. Contribution of Working Group I to the Sixth Assessment Report of the Intergovernmental Panel on Climate Change [Masson-Delmotte V, P Zhai, A Pirani, SL Connors, C Péan, S Berger, N Caud, Y Chen, L Goldfarb, MI Gomis, M Huang, K Leitzell, E Lonnoy, JBR Matthews, TK Maycock, T Waterfield, O Yelekçi, R Yu and B Zhou (eds.)]. Cambridge University Press.

Gallien TW, Schubert JE, Sanders (2011) Predicting tidal flooding in urbanized embayments: a modelling framework and data requirements. Coast. Eng. 58, 567–577.

Gallien TW, Kalligeris N, Delisle MP, Tang BX, Lucey JTD, Winters M (2018) Coastal flood modelling challenges in defended urban backshores. Geosciences 8, 450. Gallien, T.W., Sanders, B.F., Flick, R.E

Garner GG, T Hermans, RE Kopp, ABA Slangen, TL Edwards, A Levermann, S Nowikci, MD Palmer, C Smith, B Fox-Kemper, HT Hewitt, C Xiao, G Aðalgeirsdóttir, SS Drijfhout, TL Edwards, NR Golledge, M Hemer, RE Kopp, G Krinner, A Mix, D Notz, S Nowicki, IS Nurhati, L Ruiz, JB Sallée, Y Yu, L Hua, T Palmer, B Pearson (2021) IPCC AR6 Sea-Level Rise Projections. Version 20210809. PO.DAAC, CA, USA.

Gidden MJ, Riahi K, Smith SJ, Fujimori S, Luderer G, Kriegler E, van Vuuren DP, van den Berg M, Feng L, Klein D, Calvin K, Doelman JC, Frank S, Fricko O, Harmsen M, Hasegawa T, Havlik P, Hilaire J, Hoesly R, Horing J, Popp A, Stehfest E, & Takahashi K (2019) Global emissions pathways under different socioeconomic scenarios for use in CMIP6: a dataset of harmonized emissions trajectories through the end of the century. Geoscientific model development, 12(4), 1443-1475. https://doi.org/10.5194/gmd-12-1443-2019

Gudmundsson L, Bremnes JB, Haugen JE & Engen-Skaugen T (2012) Downscaling RCM precipitation to the station scale using statistical transformations–a comparison of methods. Hydrology and Earth System Sciences, 16(9), 3383-3390. https://doi.org/10.5194/hess-16-3383-2012

Gudmundsson L (2016). Package 'Qmap': statistical transformations for post- processing climate model output. The comprehensive R archive network. https:// cran.r-project.org/web/packages/qmap/qmap.pdf.

Hooijer A & Vernimmen R (2021) Global LiDAR land elevation data reveal greatest sea-level rise vulnerability in the tropics. Nature communications, 12(1), 3592. https://doi.org/10.1038/s41467-021-23810-9

Hu M, Sayama T, Zhang X, Tanaka,K, Takara K & Yang H (2017) Evaluation of low impact development approach for mitigating flood inundation at a watershed scale in China. Journal of environmental management, 193, 430-438.

IPCC (2023) AR6 Synthesis Report: Climate Change (2023) https://www.ipcc.ch/report/ sixth-assessment-report-cycle/(accessed on 30 June 2023).

Jamali B, Bach,PM, Deletic A (2020) Rainwater Harvesting for Urban Flood Management-An Integrated Modelling Framework. Water Res. 171, 115372 https:// doi.org/10.1016/j.watres.2019.115372.

Kang DH, Nam DH, Jeung SJ & Kim BS (2021) Impact assessment of flood damage in urban areas using rcp 8.5 climate change scenarios and building inventory. Water, 13(6), 756. https://doi.org/10.3390/ w13060756

Kirkpatrick J, Olbert AI (2020) Modelling the effects of climate change on urban coastal-fluvial flooding. J. Water Clim. Change. https://doi.org/10.2166/ wcc.2020.166.

Komori D, Nakamura S, Kiguchi M, Nishijima A, Yamazaki D, Suzuki S, Kawasaki A, Oki K & Oki T (2012) Characteristics of the 2011 Chao Phraya River flood in central Thailand. Hydrological Research Letters, 6, 41-46. https://doi.org/10.3178/hrl.6.41

Krysanova V, Vetter T, Eisner S, Huang S, Pechlivanidis I, Strauch M, Gelfan A, Kumar R, Aich V, Arheimer B, Chamorro A, vn Griensven A, Kundu D, Lobanova A, Mishra V, Plotner S, Reinhardt J, Seidou O, Wang X, Wortmann M, Seng X & Hattermann FF (2017) Intercomparison of regional24 scale hydrological models and climate change impacts projected for 12 large river basins worldwide—a synthesis. Environmental Research Letters, 12(10), 105002. https://doi.org/10.1088/1748-9326/aa8359

Kulp SA, Strauss BH (2019) New elevation data triple estimates of global vulnerability to sea-level rise and coastal flooding. Nature communications, 10(1), 1-12. https://doi.org/10.1038/s41467-019-12808-z

Kundzewicz ZW, Su B, Wang Y, Wang G, Wang G, Huang J, Jiang T (2019) Flood risk in a range of spatial perspectives–from global to local scales. Natural Hazards and Earth System Sciences, 19(7), 1319-1328. https://doi.org/10.5194/nhess-19-1319-2019 34

Lanzoni S, Seminara G (1998) On tide propagation in convergent estuaries. J. Geophs. Res. Oceans. 103, 30793–30812.

Li H, Zhang Y, Lei H, Hao X (2023) Machine learning-based bias correction of precipitation measurements at high altitude, Remote Sens. 15 (8), 2180.

Luo P, Mu D, Xue H, Ngo-Duc T, Dang-Dinh K, Takara K, Nover D, Schladow G (2018) Flood inundation assessment for the Hanoi Central Area, Vietnam under historical and extreme rainfall conditions. Scientific reports, 8(1), 12623. https://doi.org/10.1038/s41598-018-30024-5

Maraun D (2016) Bias correcting climate change simulations-a critical review. Current Climate Change Reports, 2(4), 211-220. https://doi.org/10.1007/s40641-016-0050-x

Mishra BK, Rafiei Emam A, Masago Y, Kumar P, Regmi RK, Fukushi K (2017) Assessment of future flood inundations under climate and land use change scenarios in the Ciliwung River Basin, Jakarta. Journal of Flood Risk Management, 11, S1105-S1115. https://doi.org/10.1111/jfr3.12311

Mtamba J, Van der Velde R, Ndomba P, Zoltán V, Mtalo F (2015) Use of Radarsat-2 and Landsat TM images for spatial parameterization of Manning's roughness coefficient in hydraulic modeling. Remote Sensing, 7(1), 836-864.

O'Brien JS, Julien PY, Fullerton WT (1993) Two-dimensional water flood and mudflow simulation. Journal of hydraulic engineering, 119(2), 244-261.

Olbert AI, Comer J, Nash S, Hartnett M (2017) High-resolution multi-scale modelling of coastal flooding due to tides, storm surges and river inflows. A Cork City example. Coast. Eng. 121, 278–296. https://doi.org/10.1016/j. coastaleng.2013.12.006.

Olesen L., L owe R, Arnbjerg-Nielsen K (2017)F lood Damage Assessment-Literature Review and Recommended Procedure. Cooperative Research Centre for Water Sensitive Cities, Melbourne, Australia.

QGIS Development Team. (n.d.) (2024) QGIS user guide. Retrieved November 9, 2024, https://docs.qgis.org/3.34/en/docs/user_manual/index.html Ramirez-Villegas, J., Challinor, A. J., Thornton, P. K., & Jarvis, A. (2013). Implications of regional improvement in global climate models for agricultural impact research. Environmental Research Letters, 8(2), 024018.

Randall DA, and Coauthors (2007) Climate models and their evaluation. Climate Change 2007: The Physical Science Basis, S. Solomon et al., Eds., Cambridge University Press, 589–662.

Riahi K, Van Vuuren DP, Kriegler E, Edmonds J, O'neill BC, Fujimori S, Bauer N, Calvin K, Dellink R, Fricko O, Tavoni, M (2017) The Shared Socioeconomic Pathways and their energy, land use, and greenhouse gas emissions implications: An overview. Global environmental change, 42, 153-168. https://doi.org/10.1016/j.gloenvcha.2016.05.009

Sanders BF (2017) Hydrodynamic modelling of urban flood flows and disaster risk reduction. Natural Hazard Science, Oxford Research Encyclopedias.

Sayama T, Tatebe Y, Tanaka S (2015) An emergency response-type rainfall-runoff-inundation simulation for 2011 Thailand floods. Journal of Flood Risk Management, 10(1), 65-78. https://doi.org/10.1111/jfr3.12147

Supharatid S (2016) Skill of precipitation projectionin the Chao Phraya river Basinby multi-model ensemble CMIP3-CMIP5. Weather and climate extremes, 12, 1-14. https://doi.org/10.1016/j.wace.2016.03.001

Supharatid S, Aribarg T, Nafung J (2021) Bias-corrected CMIP6 climate model projection over Southeast Asia. Theoretical and Applied Climatology, 147, 669-690. https://doi.org/10.1007/s00704-021-03844-1

Taylor KE (2001) Summarizing multiple aspects of model performance in a single diagram. Journal of geophysical research: atmospheres, 106(D7), 7183-7192. https://doi.org/10.1029/2000JD900719

Teutschbein C, Seibert J (2012) Bias correction of regional climate model simulations for hydrological climate-change impact studies: Review and evaluation of different methods. Journal of hydrology, 456, 1229.

Van Den Besselaar EJ, Van Der Schrier G, Cornes RC, Iqbal AS, Klein Tank AM (2017) SA-OBS: a daily gridded surface temperature and precipitation dataset for Southeast Asia. Journal of Climate, 30(14), 5151-5165. https://doi.org/10.1175/JCLI-D-16-0575.1

World Bank (2012) Thai Flood 2011, Rapid Assessment for Resilient Recovery and Reconstruction Planning, World Bank, Bangkok.

Yoshikane T, Yoshimura K (2022) A bias correction method for precipitation through recognizing mesoscale precipitation systems corresponding to weather conditions, PLoS Water 1(5) e0000016.

Zarei M, Najarchi M, Mastouri R (2021) Bias correction of global ensemble precipitation forecasts by random forest method, Earth Sci. Inform. 14, 677–689.

Zhao L, Zhang T, Fu J, Li J, Cao Z, Feng P (2021) Risk Assessment of Urban Floods Based on a SWMM-MIKE21-Coupled Model Using GF-2 Data. Remote Sens. 13 (21), 4381. https://doi.org/10.3390/rs13214381.